PAPER

Calcite formation by hydrothermal carbonation of portlandite: complementary insights from experiment and simulation

B. Fritz,[a] A. Clément,[a] G. Montes-Hernandez[b] and C. Noguera*[cd]

The present study complements experimental results of calcite nanoparticle formation by hydrothermal carbonation of calcium hydroxide by a simulation strategy, in which both the chemical evolution of the aqueous solution and the solid phases – dissolution of portlandite and nucleation and growth of secondary calcite particles – are considered. The simulation is performed with the help of the NANOKIN code. It includes a full treatment of speciation processes in the aqueous solution, a rate equation for the dissolution of primary minerals, and a full account of nucleation and growth processes during the formation of new particles. This strategy has allowed us to decipher the various steps in the mineral transformation and solution evolution. The comparison between experiment and simulation puts strong constraints on simulation parameters, while modeling can give information on *in situ* conditions, currently not often available experimentally.

I. Introduction

In natural geological systems the evolution of rocks near the surface of the Earth is highly driven by water–rock interaction processes in the water cycle between atmosphere, soils and aquifers.[1] Along this cycle, disequilibrium conditions between minerals and solutions lead to dissolution and precipitation of rock-forming minerals and it is not always easy to know precisely under which conditions mineral particles have been formed and how this correlates with their distribution of sizes.

Generating particles in the lab allows more strict control of conditions of formation and easier fundamental understanding. It may also reproduce conditions used in industrial processes. One can associate it to a simulation strategy and use it to refine models of water–rock interactions. In the line of continuing efforts to develop better and better models for water–rock interactions,[2–4] we have implemented concepts of nucleation and growth into kinetic approaches of precipitation of secondary mineral phases in our numerical codes.[1,5–8]

In this study, we have chosen to focus on an example of particle formation under well controlled conditions to complement lab experiments by a simulation strategy, namely calcite formation by hydrothermal carbonation of portlandite.

Calcite is an important ubiquitous mineral in many geochemical systems at low temperatures, such as weathering systems leading to soil formation, but also at higher temperatures in many hydrothermal systems, natural or induced by human activities (carbon sequestration, technological hindrance, scale formation, various fields of industry). Calcite may form as a product of inorganic systems or as a biomineral.[9,10] Calcium carbonate formation by synthesis in aqueous homogeneous phase has been much studied with the focus of selectively orienting the precipitation towards specific solid phases (calcite, aragonite, vaterite, ikaite or amorphous calcium carbonate), *via* control of experimental parameters, such as supersaturation value, temperature, pH, stirring velocity, initial $(Ca^{2+})/(CO_3^{2-})$ activity ratio, additives, *etc*.[11–15] In parallel, recent atomistic simulations have highlighted some specificities of this preparation procedure, such as the existence of prenucleation clusters in the aqueous solution, on a very short time scale currently inaccessible to experiments[16] and the competition between various calcium carbonates.[17]

Much less work was devoted to calcite precipitation induced by carbonation of calcium oxide or hydroxide under exposition to pure CO_2 gas or a mixture of CO_2 and H_2O gases.[18–20] Contrary to the case where H_2O vapor is present which usually produces hydrated calcium carbonates (ikaite, monohydrocalcite, amorphous calcium carbonate), it was recently shown that the synthesis route using only high CO_2 pressure under dry conditions and moderate to high temperature is a way to produce fine calcite particles,[21–25] as needed *e.g.* in industrial pharmaceutical particle engineering.[26]

[a]*Université de Strasbourg/EOST, CNRS, Laboratoire d'Hydrologie et de Géochimie de Strasbourg, 1 rue Blessig, F-67084 Strasbourg Cedex, France*
[b]*CNRS and University Joseph Fourier – Grenoble 1, Institute of Earth Sciences (ISTerre), OSUG/INSU, BP 53, 38041 Grenoble Cedex 9, France*
[c]*CNRS, Institut des Nanosciences de Paris, UMR 7588, 4 place Jussieu, 75005 Paris, France*
[d]*UPMC Univ Paris 06, INSP, UMR 7588, 4 place Jussieu, 75005 Paris, France*

The aim of this study is to complement previous experimental results of calcite nanoparticle formation by hydrothermal carbonation of calcium hydroxide by a simulation strategy allowing a better understanding of the different steps of this process. Previous work[23–25] has stressed that calcite is the main $CaCO_3$ phase produced by this method, thus rendering more straightforward the interpretation of experimental data. Modeling makes combined use of several home made simulation codes (KINDIS[3] and NANOKIN[7]), allowing an account of relevant ion speciation in the aqueous solution, dissolution, nucleation and growth processes.

The paper is organized as follows. Section II gives information on the synthesis route and the simulation methods. The main results are presented in Section III while discussion in Section IV focuses on the complementarity between experiment and modeling to provide an understanding of the mechanism of calcite formation.

II. Methods

A. Experimental

We recall here the experimental set up used for the carbonation of portlandite, as reported by one of us.[23] One liter of high-purity water with electrical resistivity of 18.2 MΩ cm and 74.1 g of commercial calcium hydroxide (provided by Sigma-Aldrich) with 96% chemical purity (3% $CaCO_3$ and 1% other impurities) are placed in a titanium reactor (autoclave with an internal volume of 2 L). The hydroxide particles are immediately dispersed with mechanical agitation (400 rpm). The dispersion is then heated to the targeted temperature (30 or 90 °C) with a heating system adapted to the reactor. When the dispersion temperature is reached, an amount of CO_2 (provided by Linde Gas S.A.) is injected in the reactor so as to reach a p_{CO_2} partial pressure of 55 bars (96.05 g at 30 °C and 80.18 g at 90 °C) and the total pressure in the system is immediately adjusted to 90 bars by argon injection. Under these P–T conditions, the vapor phase consists mainly of an Ar + CO_2 mixture with the CO_2 in a gaseous state at 30 °C and in a supercritical state at 90 °C. In order to evaluate the precipitation (or production) rate, different reaction times are considered.

The aqueous carbonation of $Ca(OH)_{2(s)}$ is an exothermic process that concerns simultaneously the dissolution of $Ca(OH)_{2(s)}$:

$$Ca(OH)_{2(s)} + 2H^+ \rightarrow Ca^{2+} + 2H_2O \qquad (1)$$
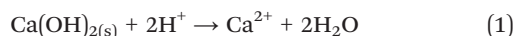
and the dissolution of CO_2 in water,

$$CO_2 + H_2O \rightarrow CO_3^{2-} + 2H^+ \qquad (2)$$
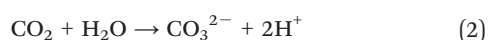
These processes produce a fast supersaturation I of solution with respect to $CaCO_3$,

$$I = \frac{(Ca^{2+})(CO_3^{2-})}{K_C} > 1 \qquad (3)$$

where (Ca^{2+}) and (CO_3^{2-}) are the activities of calcium and carbonate ions in the solution, respectively, and K_C is the solubility product of the solid phase. Then the formation of calcite particles takes place according to the reaction:

$$Ca^{2+} + CO_3^{2-} \rightarrow CaCO_3 \qquad (4)$$

Morphological analysis of the solid products is performed by SEM, with a HITACHI S-4800 microscope. X-ray powder diffraction (XRD) analyses are performed using a D5000, SIEMENS diffractometer in Bragg–Brentano geometry, equipped with a goniometer theta–theta with a rotating sample holder. The XRD patterns are collected using Cu Kα$_1$ ($\lambda_{K\alpha_1}$ = 1.5406 Å) and Kα$_2$ ($\lambda_{K\alpha_2}$ = 1.5444 Å) radiation in the range 2θ = 10–70° with a step size of 0.04° and a counting time of 6 seconds per step. Rietveld refinement of XRD patterns is carried out with the program Fullprof[27] following a standard procedure, which can be found in Montes-Hernandez *et al.*, 2009.[25]

Additionally, the pH (using MA235 pH/ion analyzer) and the calcium concentration (using ICP Perkin Elmer Optima 3300 DV) are measured in filtered solutions. For this purpose, about 25 mL of suspension are sampled in the reactor as a function of time during calcite precipitation.

B. Simulations

The simulation of calcium carbonate precipitation in the batch reactor at T = 30 or 90 °C and under constant gaseous volume conditions is performed with the help of the NANOKIN code.[5–7] It includes a full treatment of speciation processes in the aqueous solution according to a published database,[2,28] a rate equation for the dissolution of primary minerals, and a full account of nucleation and growth processes during the formation of new particles.

In the present context, rate equations of the type:

$$\frac{dM}{dt} = k(1 - I) \qquad (5)$$

are used to account for the dissolution of portlandite (according to eqn (1)) and CO_2 in water. CO_2 is described by a state equation of the van der Waals type:

$$\left(p_{CO_2} + \frac{n^2 a}{V^2}\right)(V - nb) = nRT \qquad (6)$$

in which p_{CO_2}, V, T and n are its partial pressure, volume, temperature and mole number, respectively, and R the perfect gas constant. The two corrective terms to the perfect gas equation (a the cohesion pressure, and b the co-volume) account for interactions between molecules in the liquid and gas state. Their importance decreases above the critical temperature, thus supporting the use of such an equation also in the supercritical state. The parameters $a = 27(RT_c)^2/64P_c$ and $b = RT_c/8P_c$ of the van der Waals equation are related to the critical pressure P_c and temperature T_c. In the case of CO_2, they are equal to a = 0.364 Pa m^6 mol^{-2} and b = 4.27 × 10^{-5} m^3 mol^{-1}. Simulation is performed assuming constant gaseous volume V = 1 L in the reactor, as in the experiment.

The system is closed, so that there is conservation of the total amount of carbon (including gaseous CO_2, aqueous species CO_3^{2-}, HCO_3^- and H_2CO_3, $CaCO_{3(aq)}$, $CaHCO_3^+$, $NaCO_3^-$ and carbon contained in the $CaCO_3$ solid phase) and of the total amount of calcium (calcium contained in the portlandite solid phase, the aqueous species $CaCO_{3(aq)}$, $CaHCO_3^+$, $Ca(OH)^+$ and Ca^{2+} and calcium contained in the calcium carbonate solid phase).

The treatment of precipitation relies on the theoretical approach of nucleation, growth and/or resorption of particles of fixed composition in aqueous solutions at constant temperature that we have developed in the past.[5–7] The supersaturation state I of the aqueous solution with respect to the newly formed phase is the driving force for precipitation when $I > 1$. The method combines the classical theory of particle nucleation[29,30] with size dependent kinetic rate laws for particle growth and/or resorption. The relationship between the particle volume V, their number of formula units n, their molecular volume v and their edge length l is written as $V = nv = fl^3$, with f a form factor.[31] As a function of I, the size of the critical nuclei and the nucleation barrier thus read (σ the mean surface energy and k_B related to R and the Avogadro number $k_B = R/N_{Av}$):

$$n^* = \frac{2u}{\ln^3 I}; \quad \frac{\Delta G^*}{k_B T} = \frac{u}{\ln^2 I} \quad \text{with } u = \frac{32 f v^2}{(k_B T)^3} \qquad (7)$$

The nucleation rate F is assumed to be an activated quantity with respect to the nucleation barrier, with a constant pre-factor F_0:

$$F = F_0 \, \exp\left(-\frac{\Delta G^*}{k_B T} \right) \qquad (8)$$

Once formed and as the saturation state of the solution evolves with time, the particles experience growth or resorption, depending upon the relative value of their size and the instantaneous critical nucleus size.

$$\frac{dl}{dt} = \kappa \left[I - \exp\left(\frac{2u}{n} \right)^{1/3} \right] \qquad (9)$$

From this, the time dependence of the size n of the particle is obtained, which can be written under the general form (t_1 the time of formation of the critical nucleus, t the instantaneous time):

$$n(t_1,t) = \frac{2u}{\ln^3 I(t_1)} + \frac{3\kappa f^{1/3}}{v^{1/3}} \int_{t_1}^{t} n^{2/3}(t_1,t') \left(I(t') - \exp\left[\frac{2u}{n(t_1,t')} \right]^{1/3} \right) dt' \quad (10)$$

Finally, in the closed system upon consideration, nucleation and growth exert a feed-back effect on the aqueous solution modifying its saturation state. At time t, the total number $N(t)$ of $CaCO_3$ growth units that have changed phase is equal to:

$$N(t) = \int_0^t F(t_1)(n(t_1,t) - 1)dt_1 \qquad (11)$$

From the knowledge of $N(t)$, the amount of dissolved CO_2 and portlandite, the conservation equations for calcium and carbon and the electric neutrality, it is possible to estimate the activity of all ions in solution, using an aqueous speciation model, and thus deduce the value of the saturation state I at the next time step. The instantaneous value of the saturation index of the solution $I(t)$ is the key parameter that drives the size evolution of stable/unstable particles and the model keeps track of all particles in the system.

Additionally, with a less refined description of the precipitated phase, starting from a given state of the aqueous solution, it is possible to simulate a change of pressure or a change of temperature, using the KINDIS code,[3,32] thus allowing a connection between *in situ* simulations and *ex-situ* measurements.

III. Results

As proved in previous studies that followed the same experimental protocol,[23–25] by the record of XRD patterns with Rietveld refinements and TEM images, the unit cell parameters of the solid phase remain practically constant during growth, being those of calcite. Small amounts of other anhydrous $CaCO_3$ polymorphs (vaterite or aragonite), or hydrated calcium carbonates (ikaite, monohydrocalcite or hydrated amorphous calcium carbonate) have not been detected by conventional tools (XRD, TGA, FTIR), which puts a higher limit of ~1% and ~5%, respectively, to their possible amount mixed with calcite, at least after the first structural measurement (15 min). For these reasons, we consider that calcite is the dominant phase formed under the present experimental conditions, and will be the unique solid phase allowed to precipitate in the NANOKIN simulation.

Fig. 1a–d display the time evolution of the relevant gas, solution and solid phase characteristics, obtained from experiment and simulation: amount of dissolved CO_2 and portlandite, amount of precipitated calcite, mean calcite particle size, concentration of calcium and pH in solution.

A few comments are useful regarding experimental results. As a function of time during calcite precipitation, small amounts of solution are sampled in the reactor and filtered. The time evolution of the portlandite and calcite amounts is thus obtained. Concerning the calcium concentration and pH, they are measured after full degassing ($p_{CO_2} \approx 10^{-3.5}$ atm) and equilibration at ambient temperature $T = 22.5$ °C. For these two quantities, experimental points in Fig. 1(d and e) are thus *ex-situ* measurements, while simulation points represent the *in situ* state of the aqueous solution at the temperature and CO_2 pressure inside the reactor. In Section IV, we will discuss the relationship between both sets of data and the information they provide.

Table 1 presents the values of the parameters entered in the simulation. The solubility products were taken from ref. 28. The portlandite dissolution rate k_P was calculated as the product of the total portlandite area (specific surface area in the experiment is 16 m^2 g^{-1}) times the dissolution constant
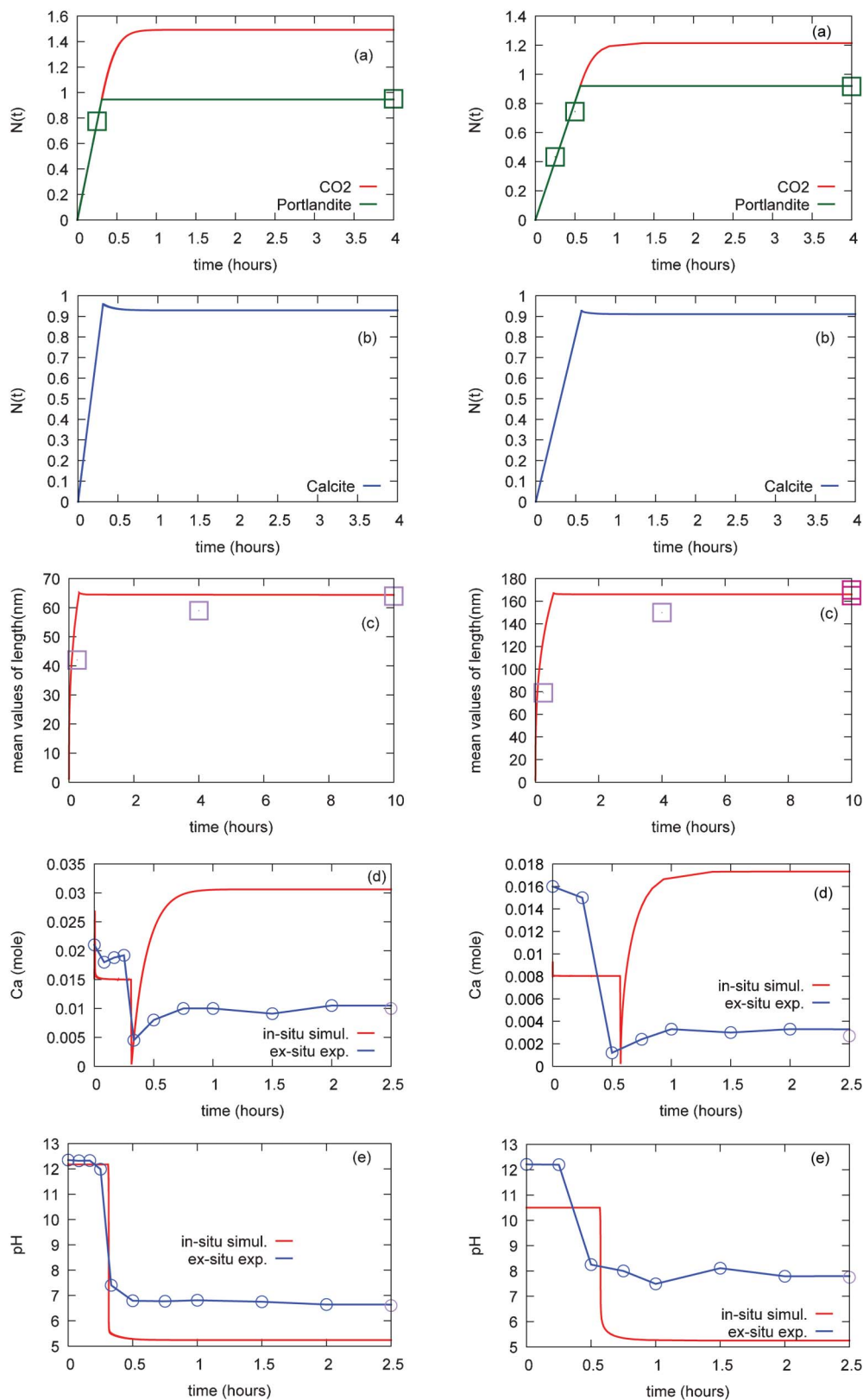
Fig. 1 Left column: 30 °C data. Right column: 90 °C data. (a) Time evolution of the amount of dissolved CO_2 (red curve) and portlandite (green curve). (b) Time evolution of the amount of precipitated calcite. (c) Time evolution of the mean calcite particle size. Squares are *ex-situ* experimental points and, when red, correspond to measurements at 24 and 48 hours. (d) Time evolution of calcium concentration in solution. (e) Time evolution of pH. Blue dots are *ex-situ* experimental points, red lines are *in situ* simulation results; the time range has been restricted to 2.5 hours, since no visible further evolution is found beyond that time.

quoted by Bullard *et al.*[35] (as inferred from ref. 36), renormalized by temperature effects, with an activation enthalpy of 57.5 kJ mol^{-1}.[35] We will see in Section IV that the precise value of k_P is unimportant because portlandite dissolution is limited by the CO_2 dissolution rate k_{CO_2}. Not finding published values for the latter, we adjusted it to obtain the correct slope for the short term time evolution of the dissolved portlandite and CO_2 amounts (Fig. 1a). As regards calcite rhombohedral particles, we take the mean surface energy $\sigma = 0.097$ J m^{-2} tabulated by Nielsen and Söhnel.[33] The value of the prefactor of nucleation frequency F_0 is unknown and kept as an adjustable parameter. In a first step, the calcite growth constant κ is adjusted in such a way that calcite particles have the correct long term mean size (Fig. 1b). We will show in Section IV that the values written in Table 1 are consistent with earlier reports.[37–39]

From Fig. 1, calcite formation by hydrothermal carbonation of portlandite appears to take place in two distinct stages. Up to a critical time t_c ($t_c \approx 0.33$ h at $T = 30$ °C and $t_c \approx 0.7$ h at $T = 90$ °C), portlandite and CO_2 dissolve nearly proportionally to time and in equal amounts (number of moles). Calcite starts precipitating very early (less than two seconds), as soon as the critical supersaturation is reached and its amount is equal to the number of moles of portlandite which is dissolved. Aside from some fast variations at very short times (not recorded experimentally), pH and the calcium concentration in solution remain constant during this whole phase. t_c represents the time at which portlandite has been totally dissolved.

Beyond t_c, there is a sudden drop of pH, which can be related to the pursuing dissolution of the excess of CO_2 in the gas phase. This induces a tiny redissolution of calcite, which however translates in a strong rise of calcium concentration in the aqueous solution. The mean calcite particle size, on the other hand, stops growing. The ageing process is starting.

IV. Discussion

While the previous section has demonstrated a good agreement between experimental measurements and simulation results, we now wish to discuss how such an agreement has been reached, what are the constraints that experimental data provide on the simulation parameters and what is the complementary information that simulation brings with respect to experiment. We will close this section by summarizing the information gained on the mechanism of calcite formation by hydrothermal carbonation of portlandite.

A. Sensitivity to simulation parameters

In the first step of preparation of the experiment, one mole of portlandite is introduced in the reactor and equilibrated with a pH = 7 aqueous solution, prior to the carbonation process. The starting pH and C_{Ca} values are thus only dependent on the solubility product of portlandite K_P. This explains why measurements (always done at $T = 22.5$ °C) find the same pH values and the same C_{Ca} values, whether the solution is withdrawn from the $T = 30$ °C or the $T = 90$ °C batch. Since K_P

Table 1 Parameters used in the simulation: solubility products K and dissolution rates k for portlandite[46] (P) and CO_2; solubility product K and growth constant κ for calcite (C). The prefactor F_0 of calcite nucleation frequency is taken equal to 10^{28} particles per liter per second; its mean surface energy[33] is $\sigma = 0.097$ J m^{-2}, its molecular volume[34] is $v = 6.13 \, 10^{-29}$ m^3 and the $(10\bar{1}4)$ rhombohedral form factor $f = 0.978$

	$T = 22.5$ °C	$T = 30$ °C	$T = 90$ °C
log K_P	22.75	22.177	18.55
k_P (mol L^{-1} s^{-1})		12.45×10^{-3}	543×10^{-3}
log K_{CO_2}	-18.152	-18.129	-18.362
k_{CO_2} (mol L^{-1} s^{-1})		0.85×10^{-3}	0.45×10^{-3}
log K_C		-8.511	-9.171
κ (m s^{-1})		1.35×10^{-12}	6.5×10^{-11}

decreases at increasing temperatures, the experimental values (pH = 12.35 and C_{Ca} = 21 mmol L^{-1}) are larger than those issued from simulations (pH = 12.2 and C_{Ca} = 15.2 mmol L^{-1} at $T = 30$ °C and pH = 10.5 and C_{Ca} = 8 mmol L^{-1} at $T = 90$ °C).

According to the k_P value reported in Table 1, the total dissolution of one mole of portlandite would require less than two minutes. Rather, it takes a fraction of an hour, thus showing that dissolution is limited by the amount of protons provided by the dissolution of CO_2 (eqn (2)). The knowledge of the characteristic time t_c for total dissolution of portlandite, obtained in the experiment, thus allows determination of the dissolution rate k_{CO_2} of CO_2 under the present experimental conditions, in an unambiguous way (Table 1). k_{CO_2} is found to be in the range 10^{-4}–10^{-3} mol s^{-1}, *i.e.* roughly 15 times smaller than k_P at $T = 30$ °C and 1200 times smaller at $T = 90$ °C. Playing with the parameters k_P and k_{CO_2}, we found that, for all values of $k_P > 2k_{CO_2}$, simulation reproduces all experimental findings in the first stage of calcite formation. If this inequality is not fulfilled, the pH of the solution immediately tumbles down in the acidic range. We can thus conclude that, for $t < t_c$, being able to reproduce the experimental results gives a strong constraint on the value of k_{CO_2}, but not on k_P, provided that $k_P > 2k_{CO_2}$. The values of k_P that we have deduced from the literature, written in Table 1, are consistent with this inequality.

Due to the importance of calcite, many attempts have been made to simulate this material and its surfaces, mainly based on atomistic classical force fields.[40] The most advanced one,[41] which includes temperature effects, predicts a value of ~ 0.4 J m^{-2} for the energy of the $(10\bar{1}4)$ surface in contact with water, which, if confirmed, would prevent any possibility of calcite precipitation under most experimental conditions. However, because the force field is non-reactive, it omits water dissociation effects as well as surface charging. In a number of cases, partial hydroxylation is known to significantly stabilize surfaces in contact with water.[42,43] Similarly, relying on experimental results combined with first principles simulations on boehmite, it has been proved, on general grounds, with the help of the MUSIC model,[44] that surface charges, associated with pH values away from the point of zero charge, are efficient to decrease the interfacial surface energy of materials.[45] While the importance of such effects has not been quantified in the case of calcite, it is likely that the value
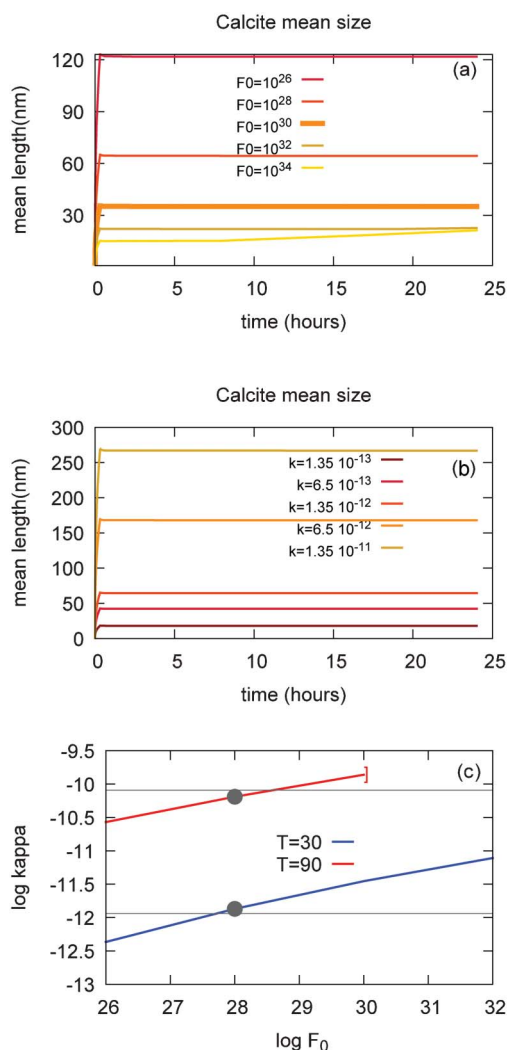
Fig. 2 Characteristics of calcite mean particle size at $T = 30$ °C for different values of (a) the nucleation frequency prefactor F_0, and (b) the calcite growth constant κ; (c) Calcite nucleation parameters κ and F_0 allowing a good account of the maximum particle sizes at $T = 30$ °C and $T = 90$ °C.

0.4 J m^{-2} is significantly overestimated. At the present stage of knowledge, we have thus relied on the experimental value 0.097 J m^{-2} quoted by Nielsen and Söhnel.[33]

Considering the correlation between the amount of precipitated calcite and that of dissolved portlandite in the first stage of the experiment, the rate of calcite precipitation appears to be limited by the rates of CO_2 and portlandite dissolution, *i.e.* by the concentrations of Ca^{2+} and CO_3^{2-} ions available in solution, rather than by its own nucleation frequency and/or growth constant. The maximum value of the mean particle size, on the other hand, is strongly dependent on these parameters, as shown in Fig. 2a and b. As could have been expected, it is an increasing function of κ and a decreasing function of F_0. This anti-correlation between κ and F_0 reflects the fact that, for $t > t_c$, the precipitate contains a constant amount of calcite (approximately one mole), but which can contain a small number of big particles or many small particles. Additionally, simulations reveal

(Fig. 2a) that F_0 should not exceed some critical value, otherwise, for a given κ, the mean particle size keeps increasing beyond t_c in disagreement with experiment.

Experimental results thus put some constraints on the acceptable values for the (F_0, κ) pair to be entered in the simulation, but do not allow to fix them separately in an unequivocal way. Fig. 2c shows the values that yield a good account of the calcite particle maximum sizes found experimentally at $T = 30$ °C and $T = 90$ °C. The two sets of values are located on nearly straight lines in the log–log plot and terminate at some F_0 value beyond which the mean particle size does not remain constant at $t > t_c$. The simulation results given in Section III have been obtained by choosing (F_0, κ) parameter pairs on these plots with $F_0 = 10^{28}$ particles per second per liter, independently of the temperature. They are represented by dots in Fig. 2c.

The κ values deduced from this procedure (see Table 1) are consistent with literature data, although a strict comparison is not an easy task since calcite growth constant κ depends on temperature, pH and p_{CO_2}, and since the two latter (especially p_{CO_2}) vary continuously in the present experiment. Relying on the value of κ measured at $T = 20$ °C in ref. 37, $\kappa = 0.47 \times 10^{-8}[H^+]^{0.318}(I - 1)$ m s^{-1}, and on the activation enthalpy for growth found equal to 46 kJ mol^{-1},[38] it is possible to infer $\kappa = 1.15 \times 10^{-12}$ m s^{-1} for the pH condition relevant when $T = 30$ °C (pH = 12.2) and $\kappa = 8.14 \times 10^{-11}$ m s^{-1} for the pH condition relevant when $T = 90$ °C (pH = 10.5). These values are also reported in Fig. 2c as horizontal lines. They appear to be reasonably close to those entered in the simulation.

B. State of the aqueous solution: comparison experiment-simulation

While it is possible to make a direct comparison between experiment and simulation results for portlandite and CO_2 dissolution, total calcite precipitate and mean particle size, because the conditions under which measurements are made are close to *in situ* conditions, the same is not true for the time evolution of the aqueous solution characteristics. Measuring pH and element concentrations *in situ* would require very specific equipment, presently not available in our teams. Measurements have been made at ambient temperature $T = 22.5$ °C after filtering and degassing, which can considerably change the state of the aqueous solution, in particular the pH. An example was given in Section IV A for the pH measurement at time $t = 0$. A similar situation occurs at time $t = 48$ h (when calcite is close to equilibrium with the aqueous solution), where pH ≈ 5 in *in situ* conditions ($T = 30$ °C and $p_{CO_2} \approx 16$ bars) while pH ≈ 7 in *ex-situ* conditions ($T = 22.5$ °C and $p_{CO_2} \approx 10^{-3.5}$ bars), a difference that temperature dependence of the calcite solubility and carbon speciation in solution and p_{CO_2} values straightforwardly explain.

At intermediate times, a quantitative one-to-one comparison is not possible because the system is strongly out-of-equilibrium. It can be said that, qualitatively, the change of regime at t_c is clearly marked on the pH and C_{Ca} time evolutions both in the *ex-situ* and *in situ* data (Fig. 1c and d). This illustrates the limit of the comparison exercise as long as there is no access to experimental *in situ* values for chemical controls on the solution. In this regime, modeling appears a
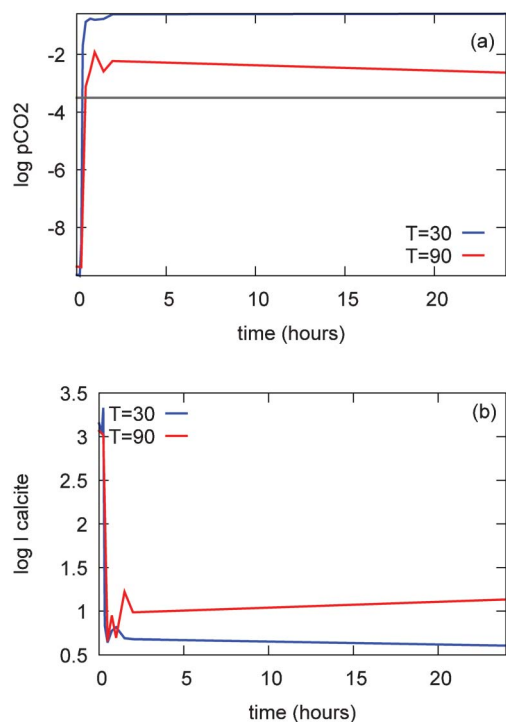
Fig. 3 Saturation tests of the experimental aqueous solution thermodynamic state after degassing and cooling (code KINDIS). Top panel: log p_{CO_2} as a function of time for the two experiments, and reference to the ''ideal'' ambient condition $p_{CO_2} = 10^{-3.5}$ bars. Lower panel: saturation state of the aqueous solution with respect to calcite.

precious complement to experiment to provide information on what happens *in situ* and to help decipher the mechanisms of precipitation (see Section IV C).

Additionally, modeling can also provide information on some difficulties associated with experiment, in particular the degassing procedure. When sampled in the reactor, the solution is far from equilibrium with atmospheric p_{CO_2}. For example, at $T = 30$ °C in *in situ* conditions, according to NANOKIN simulation, p_{CO_2} decreases monotonically from 55 bars ($t = 0$ s) to 16 bars ($t = 48$ h). A full return to equilibrium would probably need a long time and be difficult to detect. Performing a saturation test of the measured aqueous solution thermodynamic state with the help of the KINDIS code[3] yields the results shown in Fig. 3. It clearly appears that the p_{CO_2} with which the *ex-situ* solution was in equilibrium was very low compared to *in situ* conditions, but equilibrium with atmospheric p_{CO_2} was not yet reached. Additionally, under these conditions, this analysis yields the value of the saturation state of the aqueous solution with respect to calcite, which is not directly accessible for measurement. As expected, the aqueous solution is supersaturated at all intermediate times, under the conditions of measurement. However, this raises the possibility that some calcite particles nucleate or grow during degassing, with implications for the concentration of calcium in solution, which can thus further depart from its *in situ* value. This clearly shows that *ex-situ* measurements made in a dynamic system still in evolution may be difficult to interpret, since an (often) incomplete return to equilibrium with respect

to CO_2 and a possible calcite precipitation during degassing can strongly influence the pH and the calcium concentration in solution.

C. Mechanism of precipitation

From the previous discussions, we saw how combining experiment and modeling can account for a complex process like calcite formation by carbonation of calcium hydroxide. Experiment provides some rich information, which helps to fix the parameters of the modeling. The latter complements the experiment when *in situ* measurements are not possible and allows to go deeper in the understanding of the process, thanks to the more extensive outputs it provides (at each time, all saturation states, all concentrations and activities in solution, *in situ* p_{CO_2}, crystal size distributions). We will now use this information issued from simulation to analyze in detail calcite formation.

The first stage of the process ($t < t_c$) is characterized by a concerted dissolution of CO_2 and portlandite, although their dissolution constants are largely different (Section IV A). Actually, the dissolution of each solid $Ca(OH)_{2(s)}$ formula unit requires two protons which are provided by the dissolution of one CO_2 molecule:

$$CO_2 + H_2O \rightarrow CO_3^{2-} + 2H^+$$

$$Ca(OH)_{2(s)} + 2H^+ \rightarrow Ca^{2+} + 2H_2O \quad (12)$$
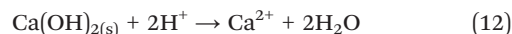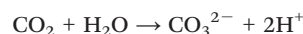
The amount (number of moles) of dissolved portlandite thus cannot exceed that of dissolved CO_2. Actually both turn out to be equal because the portlandite dissolution rate is large enough to drain the proton production in solution. CO_2 dissolution is thus the limiting step at $t < t_c$.

Additionally, since as many protons are produced by dissolution of CO_2 as consumed by dissolution of portlandite, the aqueous solution is buffered and the pH remains high and constant, as long as some portlandite remains available.

As more and more CO_2 and portlandite are dissolved, the calcium carbonate ionic activity product $Q = (Ca^{2+})(CO_3^{2-})$ increases. Its variations display a very rapid increase during the first minute, followed by a rapid then progressive decrease (Fig. 4). As demonstrated in a previous work,[6] only particles nucleated during the time interval when $dI/dt > 0$ survive in the long term. They are thus created at the very start of the carbonation process and this has implication on the shape of the crystal size distribution function (CSD; see below).

One can notice that the maximum saturation state of the aqueous solution with respect to calcite is high, of the order of 2000 at $T = 30$ °C and 300 at $T = 90$ °C. Other more soluble calcium carbonates thus also become supersaturated[47] (Table 2). In this study, we have only considered the possibility of calcite formation on the basis of X-ray diffraction characterization, which does not bring evidence of significant amount of calcium carbonate phases formed other than calcite. However, one cannot exclude the possibility that some of them act as precursors for calcite precipitation, but only at the very beginning of the carbonation process and in very small amounts.
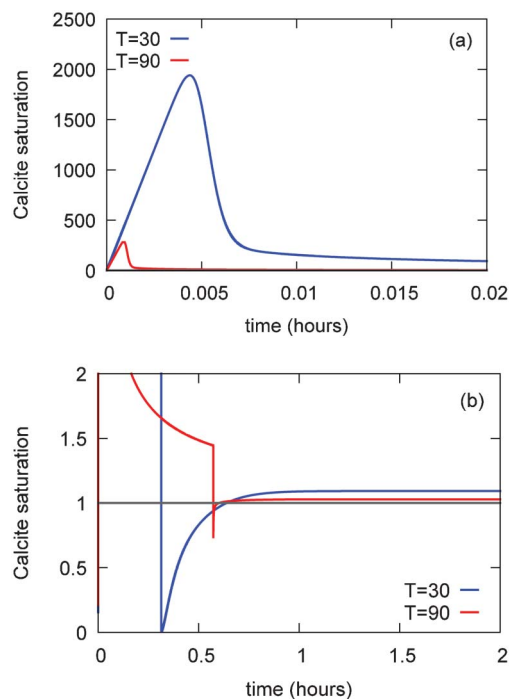
Fig. 4 Time evolution of the saturation state of the aqueous solution I with respect to calcite at $T = 30$ °C and $T = 90$ °C. (a) General shape; (b) enlargement in the saturation region $0 < I < 2$ to highlight the time interval when calcite gets under-saturated.
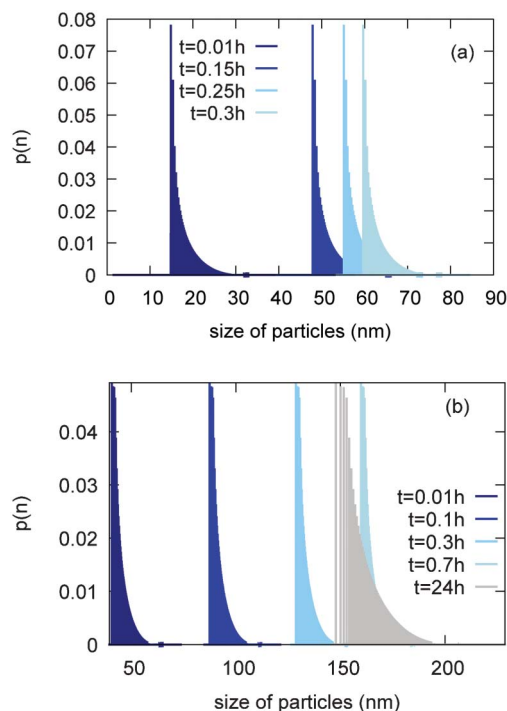

Fig. 5 (a) Calcite crystal size distribution functions during precipitation at $T = 30$ °C, taken at four different times: $t = 0.01, 0.1, 0.2$ and 0.3 h. (b) Calcite crystal size distribution functions during precipitation at $T = 90$ °C, taken at four different times: $t = 0.01, 0.1, 0.3, 0.7$ and 24 h.

When portlandite is no longer available in the reactor ($t = t_c$), the sudden drop of pH induces a sharp decrease in CO_3^{2-} activity, which leads to calcite undersaturation (Fig. 4b). Some (slight) dissolution of calcite thus results, as revealed by the decrease of the total amount of precipitate, Fig. 1a. Eventually, the Ca^{2+} activity rises again, more ($T = 90$ °C) or less ($T = 30$ °C) quickly, and the calcite saturation state I becomes larger than 1.

The calcite crystal size distribution function (CSD), as obtained with the NANOKIN code, is reported in Fig. 5 at different times. At short times, its center of gravity shifts to larger size values without much width change. After $t > t_c$ the position of the CSD center of gravity no longer changes, but its width very slowly increases. Larger particles grow at the expense of smaller ones, as characteristic of an Ostwald ripening process. The CSD shape is very asymmetric with an obvious right skew. We checked that this remains true at all times experimentally accessible ($t = 48$ h), although, eventually, in a much longer term, thermodynamic equilibrium has

Table 2 Ratio between the solubility products of some calcium carbonates and that of calcite at two temperatures $T = 30$ °C and $T = 90$ °C (from ref. 47)

Calcium carbonates	$T = 30$ °C	$T = 90$ °C
Aragonite	1.3	1.4
Vaterite	3.4	2.8
Ikaite	97.7	6025
Amorphous	223.9	223.9

to be associated to a single surviving particle, thus a fully symmetric CSD.

The reason for the right-skewed asymmetry lies in the way particles are formed. In the process of portlandite carbonation, the solution is first undersaturated with respect to calcite and some time is necessary before I exceeds the critical saturation value ($I_c \approx 125$ at $T = 30$ °C and 40 at $T = 90$ °C) at which the nucleation frequency becomes larger than one particle per second and H_2O liter. As I grows (Fig. 4a), the first few big particles are produced (small I values induce high nucleation barriers and large critical nucleus sizes, eqn (7)), then smaller and smaller particles in larger and larger amounts. After I has passed through its maximum value and in the time range when $dI/dt < 0$, particles may still be nucleated but, as shown by us previously,[6] they quickly redissolve. The shape of the CSD reflects this process: on its left side, the smallest particles are the most numerous: they were formed at times when I was close to its maximum value. On the CSD right side, the largest particles are less numerous. They were formed when I just exceeded I_c. A similar CSD shape was found in our study of kaolinite precipitation as a result of granite dissolution, in which the saturation state of the aqueous solution with respect to kaolinite displayed a similar shape.[7] Interestingly, such CSD shapes resemble the log–normal distributions of nano particles often recorded in the natural environment.[48]

V. Conclusion

We have presented a comparison between two approaches of calcite nano-particle formation: one by experimental hydrothermal carbonation of portlandite, and the other by numerical simulation of the same process. In this comparison, we have considered both the chemical evolution of the aqueous solution and the solid phases, dissolution of portlandite and nucleation and growth of secondary calcite particles. The general steps in the mineral transformation and solution evolution are found to be very comparable: initial portlandite equilibrium with the solution at high pH, dissolution of portlandite when CO_2 is introduced in the reactor and precipitation of calcite from that solution, pH drop after total portlandite consumption due to the excess of CO_2 which induces a small re-dissolution of calcite, long term Ostwald ripening of calcite particles.

With regards to the solid phases, the experiments unambiguously show the formation of calcite as major product of the hydrothermal carbonation process. The amounts of precipitated calcite and of dissolved portlandite are directly related through the mass balance of calcium, since CO_2 gas is available in excess and all the portlandite can be transformed into calcite. The comparison between experiment and simulation allowed (1) to determine the CO_2 dissolution rate k_{CO_2}, (2) to assign a minimum value for the portlandite dissolution rate $k_P > 2k_{CO_2}$, (3) to put strong constraints on the (F_0, κ) kinetic parameters for the calcite nucleation and growth. Additionally, simulation provides detailed information on the calcite particle population, the time evolution of its mean size and of the size distribution function.

Concerning the aqueous solution, such a direct comparison is not straightforward because of different thermodynamic conditions under which experiment measurements and simulation are performed. While modeling simulates *in situ* conditions (high temperature, high pressure), in the experiment, the chemical information concerning the fluid is only available after cooling, CO_2 degassing and filtration. In this context, simulation is a very useful tool to approach the experimental *in situ* values, especially sensitive data like pH, calcium concentration, or saturation indices. In the present study, it has also allowed verifying that the solution after cooling and degassing had not yet reached equilibrium with CO_2 in the ambient atmosphere.

To conclude, we would like to recommend the complementary use of numerical modeling and experimental approaches in studies of fluid–rock interactions. As shown in the present work, modeling can help understanding what happens in aqueous solutions in terms of mineral saturations and consequent kinetics of dissolution and precipitation. It is able to describe *in situ* conditions, which is presently not often available experimentally. Of course, efforts for direct measurements of *in situ* conditions remain of utmost usefulness. Such a combined strategy leading to more efficient simulations of water–rock interactions may result crucial to address topics of societal importance, like safety assessment of geological storage (CO_2, nuclear wastes) or prediction of long term evolution of geothermal systems.

References

1 *Thermodynamics and Kinetics of Water–Rock Interaction*, ed. E. H. Oelkers and J. Schott, *Reviews in Mineralogy and Geochemistry*, Mineralogical Society of America and Geochemical Society, 2009, vol. 70.
2 H. C. Helgeson, T. H. Brown, A. Nigrini and T. A. Jones, *Geochim. Cosmochim. Acta*, 1970, **34**, 455.
3 B. Madé, A. Clément and B. Fritz, *Comput. Geosci.*, 1994, **20**(9), 1347.
4 C. I. Steefel and P. Van Cappellen, *Geochim. Cosmochim. Acta*, 1990, **54**, 2657.
5 C. Noguera, B. Fritz, A. Clément and A. Baronnet, *J. Cryst. Growth*, 2006, **297**, 180.
6 C. Noguera, B. Fritz, A. Clément and A. Baronnet, *J. Cryst. Growth*, 2006, **297**, 187.
7 B. Fritz, A. Clément, Y. Amal and C. Noguera, *Geochim. Cosmochim. Acta*, 2009, **73**, 1340.
8 B. Fritz and C. Noguera, *Rev. Mineral. Geochem.*, 2009, **70**, 371.
9 P. M. Dove and J. R. M. F. Hochella, *Geochim. Cosmochim. Acta*, 1993, **57**, 705.
10 H. Y. Li, H. L. Xin, D. A. Muller and L. A. Estroff, *Science*, 2009, **326**, 1244.
11 L. Moore, J. D. Hopwood and R. J. Davey, *J. Cryst. Growth*, 2004, **261**, 93.
12 Y. Fujita, G. D. Redden, J. Ingram, M. M. Cortez, G. Ferris and R. W. Smith, *Geochim. Cosmochim. Acta*, 2004, **68**, 3261.
13 S. J. Freij, A. Godelitsas and A. Putnis, *J. Cryst. Growth*, 2005, **273**, 535.
14 L. A. Gower and D. A. Tirrell, *J. Cryst. Growth*, 1998, **191**, 153.
15 L. Pastero, E. Costa, B. Alessandri, M. Rubbo and D. Aquilano, *J. Cryst. Growth*, 2003, **247**, 472.
16 R. Demichelis, P. Raiteri, J. D. Gale, D. Quigley and D. Gebauer, *Nat. Commun.*, 2011, **2**, 590.
17 G. A. Tribello, F. Bruneval, C. C. Liew and M. Parrinello, *J. Phys. Chem. B*, 2009, **113**, 11680.
18 O. Cizer, C. Rodriguez-Navarro, E. Ruiz-Agudo, J. Elsen, D. Van Gemert and K. Van Balen, *J. Mater. Sci.*, 2012, **47**, 6151.
19 A. M. López-Periago, R. Pacciani, L. F. Vega and C. Domingo, *Cryst. Growth Des.*, 2011, **11**, 5324.
20 L. S. Gomez-Villalba, P. López-Arce, M. Alvarez de Buergo and R. Fort, *Appl. Phys. A: Mater. Sci. Process.*, 2011, **104**, 1249.
21 C. Domingo, J. Garcia-Carmona, E. Loste, A. Fanovich, J. Fraile and J. Gomez-Morales, *J. Cryst. Growth*, 2004, **271**, 268.
22 C. Domingo, E. Loste, J. Gomez-Morales, J. Garcia-Carmona and J. Fraile, *J. Supercrit. Fluids*, 2006, **36**, 202.

23 G. Montes-Hernandez, F. Renard, N. Geoffroy, L. Charlet and J. Pironon, *J. Cryst. Growth*, 2007, **308**, 228.

24 G. Montes-Hernandez, A. Fernandez-Martinez, L. Charlet, D. Tisserand and F. Renard, *J. Cryst. Growth*, 2008, **310**, 2946.

25 G. Montes-Hernandez, A. Fernandez-Martinez and F. Renard, *Cryst. Growth Des.*, 2009, **9**, 4567.

26 M. McHugh and V. Krukonis, *Supercritical Fluid Extraction: Principles and Practices*, Butterworth-Heineman, USA, 1994.

27 J. Rodriguez-Carvajal, http://www.ill.eu/sites/fullprof/php/tutorials.html, 2010.

28 D. L. Parkhurst and C. A. J. Appello, *User's Guide to PHREEQC (Version 2)*, U.S. Department of the Interior, U.S.G.S., 1999.

29 A. W. Adamson, *Physical Chemistry of Surfaces*, Interscience Publishers, 1960.

30 I. V. Markov, *Crystal Growth for Beginners: Fundamentals of Nucleation, Crystal Growth and Epitaxy*, World Scientific, Singapore, New Jersey, London, Hong Kong, 1995.

31 R. J. Reeder, in *Carbonates: Mineralogy and Chemistry: Reviews in Mineralogy*, ed. R. J. Reeder, Mineralogical Society of America, 1990, vol. 11, pp. 1–7.

32 B. Madé, A. Clément and B. Fritz, *C. R. Acad. Sci., Ser. II: Mec., Phys., Chim., Sci. Terre Univers*, 1990, **310**, 31.

33 A. E. Nielsen and O. Söhnel, *J. Cryst. Growth*, 1971, **11**, 233.

34 WebMineral Atlas Minéralogique, http://webmineral.brgm.fr:8003/mineraux/Main.html, 2008.

35 J. W. Bullard, E. Enjolras, W. L. George, S. G. Satterfield and J. E. Terrill, *Modell. Simul. Mater. Sci. Eng.*, 2010, **18**, 025007.

36 M. E. Tadros, J. Skalny and R. S. Kalyoncu, *J. Colloid Interface Sci.*, 1976, **55**, 20.

37 H. J. Meyer, *J. Cryst. Growth*, 1979, **47**, 21.

38 A. Gutjahr, H. Dabringhaus and R. Lacmann, *J. Cryst. Growth*, 1996, **158**, 296.

39 Ö. Nilsson and J. Sternbeck, *Geochim. Cosmochim. Acta*, 1999, **63**, 217.

40 P. Raiteri, J. D. Gale, D. Quigley and P. M. Rodger, *J. Phys. Chem. C*, 2010, **114**, 5997 and refereneces therein.

41 M. Bruno, F. R. Massaro, L. Pastero, E. Costa, M. Rubbo, M. Prencipe and D. Aquilano, *Cryst. Growth Des.*, 2013, **13**, 1170.

42 L. Giordano, J. Goniakowski and J. Suzanne, *Phys. Rev. Lett.*, 1998, **81**, 1271.

43 P. J. D. Lindan, N. M. Harrison and M. J. Gillan, *Phys. Rev. Lett.*, 1998, **80**, 762.

44 (*a*) T. Hiemstra, W. H. Van Riemsdijk and G. H. Bolt, *J. Colloid Interface Sci.*, 1989, **133**, 91; (*b*) T. Hiemstra, J. C. M. De Wit and W. H. Van Riemsdijk, *J. Colloid Interface Sci.*, 1989, **133**, 105.

45 J.-P. Jolivet, C. Froidefond, A. Pottier, C. Chanéac, S. Cassaignon, E. Tronc and P. Euzen, *J. Mater. Chem.*, 2004, **14**, 3281.

46 R. A. Robie, B. S. Hemingway and J. R. Fischer, *Geol. Survey Bull.*, 1979, **1452**, 1.

47 J. Kawano, N. Shimobayashi, A. Miyake and M. Kitamura, *J. Phys.: Condens. Matter*, 2009, **21**, 425102.

48 D. D. Eberl, V. Drits and J. Środoń, *Am. J. Sci.*, 1998, **298**, 499.